NANO LETTERS

pubs.acs.org/NanoLett

Letter

Dual-Gated Graphene Devices for Near-Field Nano-imaging

Sai S. Sunku,[#] Dorri Halbertal,[#] Rebecca Engelke, Hyobin Yoo, Nathan R. Finney, Nicola Curreli, Guangxin Ni, Cheng Tan, Alexander S. McLeod, Chiu Fan Bowen Lo, Cory R. Dean, James C. Hone, Philip Kim, and D. N. Basov*

Cite This: *Nano Lett.* 2021, 21, 1688−1693

Read Online

ACCESS | Metrics & More | Article Recommendations | Supporting Information

ABSTRACT: Graphene-based heterostructures display a variety of phenomena that are strongly tunable by electrostatic local gates. Monolayer graphene (MLG) exhibits tunable surface plasmon polaritons, as revealed by scanning nano-infrared experiments. In bilayer graphene (BLG), an electronic gap is induced by a perpendicular displacement field. Gapped BLG is predicted to display unusual effects such as plasmon amplification and domain wall plasmons with significantly larger lifetime than MLG. Furthermore, a variety of correlated electronic phases highly sensitive to displacement fields have been observed in twisted graphene structures. However, applying perpendicular displacement fields in nano-infrared experiments has only recently become possible [Li, H.; et al. *Nano Lett.* **2020**, *20*, 3106−3112]. In this work, we fully characterize two approaches to realizing nano-optics compatible top gates: bilayer MoS_2 and MLG. We perform nano-infrared imaging on both types of structures and evaluate their strengths and weaknesses. Our work paves the way for comprehensive near-field experiments of correlated phenomena and plasmonic effects in graphene-based heterostructures.

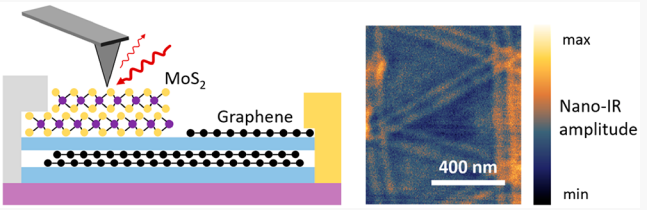

KEYWORDS: *nano-infrared imaging, nano-photocurrent, top gate, bilayer graphene*

Graphene-based van der Waals (vdW) heterostructures display a variety of phenomena including superior plasmonic properties,[1−4] tunable band structures,[5−7] topological edge states,[8−10] and correlated phases such as superconductivity.[11,12] This large variety of electronic phases arises because the properties of graphene are strongly tunable by electrostatic gates. The optical excitations corresponding to these phases lie in the infrared range of the electromagnetic spectrum,[13] where the wavelength of light, λ_0, ranges from 1 to 100 μm. Probing such heterostructures with conventional far-field optical experiments is challenging because of their limited lateral dimensions compared to λ_0. However, tip-based scanning nano-infrared experiments can overcome the diffraction limit and achieve a spatial resolution better than 10 nm.[14]

Nano-infrared experiments have established monolayer graphene (MLG) as an excellent platform for plasmonics because of a large confinement ratio λ_0/λ_p (λ_p is the plasmon wavelength),[15−17] tunability with an external gate,[1,2] and long lifetimes for the SPPs approaching 2 ps.[3,18] While MLG is well studied, the plasmonic properties of bilayer graphene are relatively unexplored.[19] When bilayer graphene is gapped and the Fermi level lies in the gap, exotic plasmonic phenomena are predicted to occur. Gapped bilayer graphene (BLG) under photoexcitation is predicted to amplify SPPs,[20] while domain wall solitons in gapped BLG could host one-dimensional SPPs with lifetimes approaching 10^2 ps.[21]

Nano-infrared experiments have also begun to probe multilayer graphene-based Moiré systems that are known to host correlated electronic phenomena such as twisted bilayer graphene (TBG),[11] twisted trilayer graphene (TTG),[22] and twisted double bilayer graphene (TDBG).[23,24] The electronic properties of all of these systems are strongly sensitive to perpendicular displacement field. For example, the correlated insulator phases in TTG and TDBG appear only for a limited range of displacement fields.[22,23]

A perpendicular displacement field can be introduced using an evaporated metal layer or a graphite layer as a top gate in conjunction with a back gate. While transport[25] and some far-field optical experiments[26−28] can be performed on such structures, they are incompatible with nano-infrared experiments for multiple reasons. First, such layers are relatively thick (tens of nanometers), which make the underlying graphene layer inaccessible to nano-optics experiments. When the layers are made thinner, the presence of a high density of high mobility free carriers leads to plasmonic effects in the top gate,

Received: November 12, 2020
Revised: February 5, 2021
Published: February 15, 2021

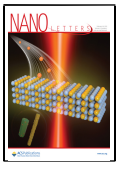

https://dx.doi.org/10.1021/acs.nanolett.0c04494
Nano Lett. 2021, 21, 1688−1693

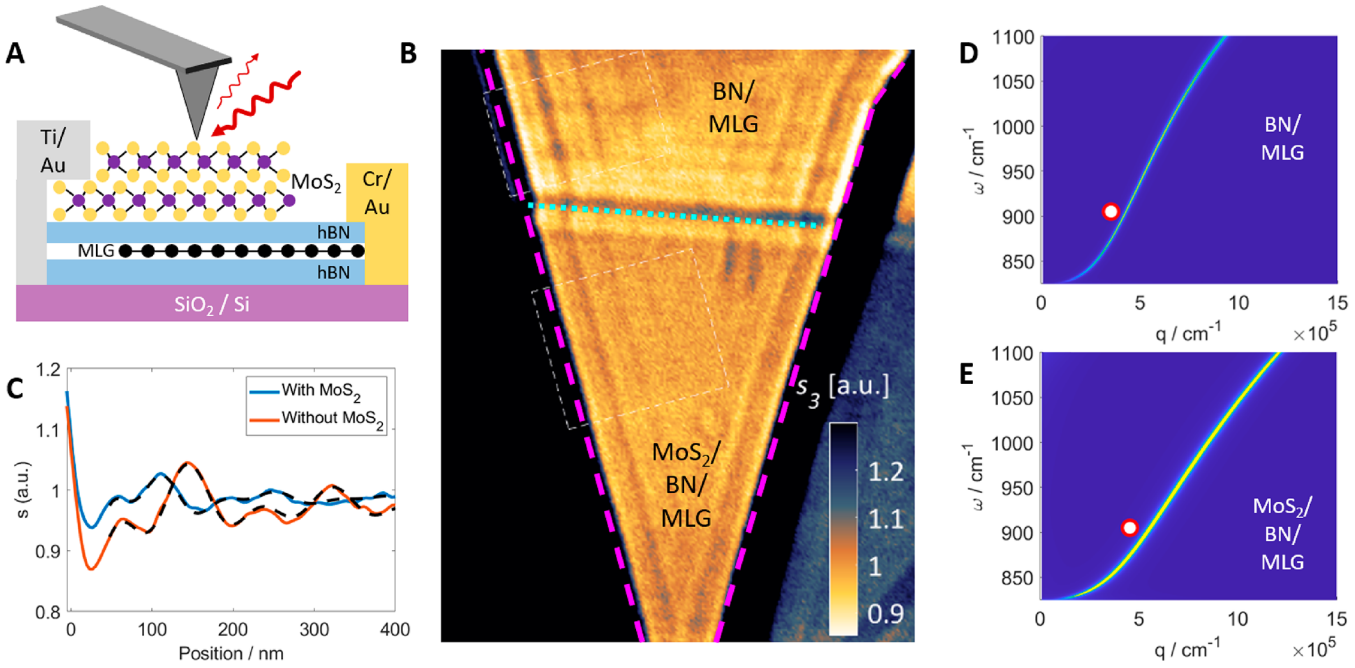

Figure 1. | Nano-optics measurements on MoS_2-gated monolayer graphene. (A) Schematic of our nano-infrared experiment and our device. Bilayer MoS_2 is contacted by Ti/Au from above, while the graphene has a side contact made of Cr/Au. (B) Two-dimensional image of the nano-infrared amplitude s over our device for V_{bg} = +80 V and V_{tg} = 0 V. The edges of MLG and MoS_2 are represented by magenta dashed and green dotted lines, respectively. (C) Line profiles of the nano-infrared amplitude s across a graphene edge showing plasmon polaritons. Black dashed lines represent fits to a damped oscillations model (Section S3 of the Supporting Information). (D) Calculated imaginary part of the reflection coefficient $\mathrm{Im}(r_p)$ matching the two experimental heterostructures: (D) BN/MLG/BN/SiO_2; (E) MoS_2/BN/MLG/BN/SiO_2. The bright contour of maximal values corresponds to the plasmon mode. The circles in panels D and E correspond to experimental data extracted from panel C (Section S3 of the Supporting Information).

which modifies and obscures the behavior of the underlying graphene layer.

Recent work has shown that MLG could be used as a top gate to study Moiré patterns in vdW heterostructures.[29] However, the capabilities and limitations of the top gate were not fully explored. While ref29 showed that two-dimensional domains in a Moiré pattern could be visualized through a MLG top gate, it is not yet known if the plasmonic phenomena in the underlying graphene layer and one-dimensional features such as domain walls in BLG can be resolved. In this work, we demonstrate and fully characterize two approaches for nano-optics compatible top gates: bilayer MoS_2 and MLG. We are able to visualize the plasmons in the MLG and TBG layers underneath the MoS_2 top gate. We further demonstrate a depletion of the carrier density of the underlying graphene layers with the top gate through measurements of the plasmon wavelength and nano-infrared scattering amplitude. We then explore the use of a MLG layer as the top gate for BLG. The doped MLG layer is a robust top gate but has strong optical response at mid-infrared frequencies of its own. We therefore explore the possibility of selectively probing the underlying BLG through nano-photocurrent imaging and are able to visualize domain walls in the BLG layer. Our work paves the way for realization of fully tunable vdW devices compatible with nano-optics experiments.

Figure 1A shows a schematic of our experimental setup. Our first device consists of monolayer graphene encapsulated between hexagonal boron nitride (hBN) layers. The thickness of the top hBN layer is kept small (2 nm) to allow optical near-field access to the underlying graphene layer. A bilayer of MoS_2 is then placed on the top hBN layer for use as a top gate, while a doped silicon layer underneath the heterostructure serves as the bottom gate. We chose MoS_2 because it is expected to be transparent to mid-infrared light. We study this device using a scanning nano-infrared microscope, where incident light from a quantum cascade laser is focused onto the apex of a sharp metallic tip. We used light of frequency $\omega = 1/\lambda_0 = 905$ cm^{-1} for all experiments in this work. The amplitude s and phase ϕ of the scattered light are detected with an interferometric method.[30] The sharpness of the tip provides the momentum necessary to launch SPPs which propagate radially outward from the tip. When the SPPs encounter a physical[1,2] or electronic[31] boundary, they are reflected and form a standing wave pattern that we directly visualize.

Figure 1B shows a two-dimensional map of the nano-infrared amplitude s measured on our device with V_{bg} = +80 V and V_{tg} = 0 V. The green dotted line marks the edge of the MoS_2 layer such that the area above the line does not contain MoS_2. We observe clear fringes parallel to the edges of the MLG (marked by magenta dashed lines) throughout the image. These fringes confirm that we are able to launch and image SPPs in the MLG layer even when the MLG is underneath MoS_2.

A comparison of the fringes above and below the MoS_2 boundary in Figure 1B indicates that the plasmon wavelength is smaller in the region with MoS_2. In Figure 1C, we plot the line profiles extracted across the graphene edge from both regions. The line profiles confirm that the plasmon wavelength is reduced to 138 nm under the MoS_2 layer (blue line in Figure 1C) compared to 177 nm without MoS_2 (orange line in Figure 1C). This reduction is due to the large static dielectric constant of MoS_2 and the resulting screening. This change in plasmon

https://dx.doi.org/10.1021/acs.nanolett.0c04494
Nano Lett. 2021, 21, 1688−1693

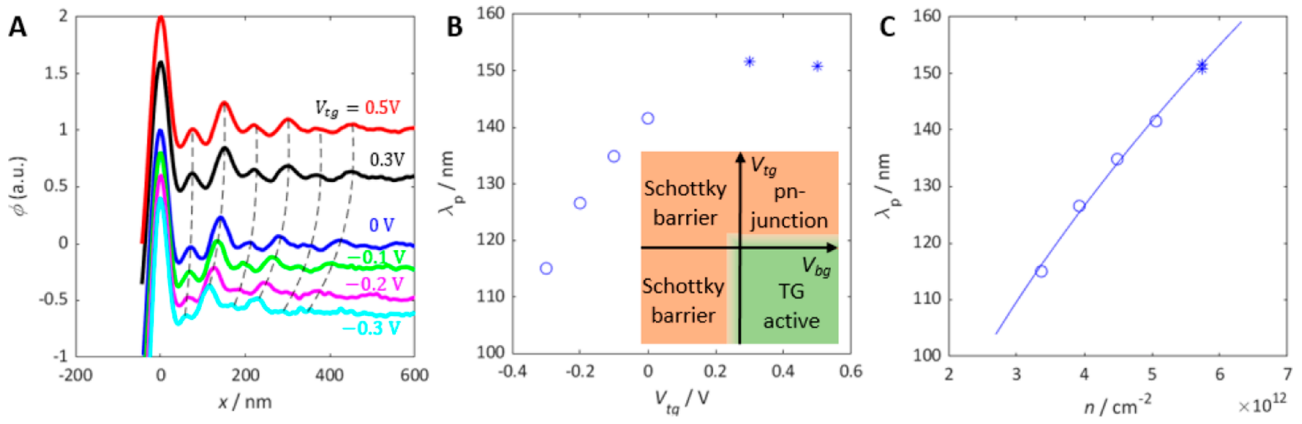

Figure 2. Carrier density modulation in monolayer graphene with MoS_2top gate. (A) Line profiles of the nano-infrared phase ϕ for various values of V_{tg} at V_{bg} = +80 V, showing a clear change in the plasmon wavelength. The curves are scaled and shifted for clarity. Dashed lines follow the plasmonic peaks and are used to extract λ_p. (B) Plasmon wavelength as a function of the top-gate voltage, V_{tg}. Circles represent $V_{tg} \leq 0$ V, and asterisks represent $V_{tg} > 0$ V. Inset shows the behavior of the MoS_2 top gate for various V_{tg} and V_{bg} values. The top gate is most effective in one of the four quadrants, and its performance decays quickly in other quadrants. (C) λ_p as a function of the estimated carrier density in the graphene layer n. The data points for $V_{tg} > 0$ V cluster together because the top gate is ineffective (described in text).

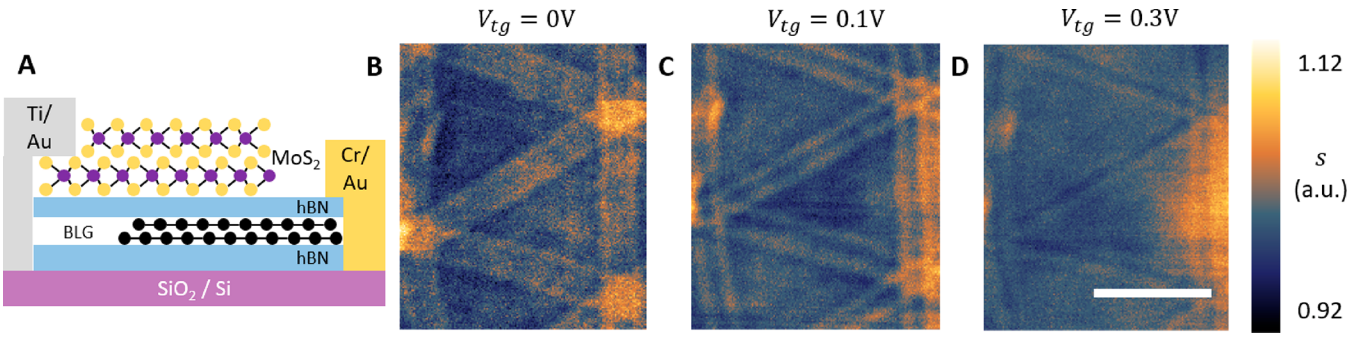

Figure 3. Demonstration of top-gating effect in bilayer graphene domain walls. (A) Schematic of the heterostructure. (B, C, D) Nano-infrared amplitude image of domain walls in BLG for three different top-gate voltages with V_{bg} = +80 V. Scale bar 400 nm.

wavelength is consistent with the calculated change in plasmon dispersion (Figure 1D,E).

Figure 2 demonstrates the tuning of carrier density in the MLG layer with the MoS_2 top gate. Figure 2A shows line profiles of the nano-infrared phase ϕ for different values of top-gate bias, V_{tg}, for a fixed value of back-gate bias, V_{bg} = +80 V. We observe a clear change in the plasmon wavelength as V_{tg} is changed. At negative values of V_{tg}, we observe a decrease in the plasmon wavelength which is consistent with a depletion of the carrier density in the graphene layer. When V_{tg} is tuned to +0.3 V, we observe an increase in λ_p. But a further increase in V_{tg} to +0.5 V does not change λ_p, indicating that the carrier density in MLG does not change (Figure 2B,C). This limitation is the result of a pn-junction forming in the MoS_2 layer as described below. Taken together, our results confirm that we are able to deplete the carrier density in the graphene layer which is necessary for realizing gapped BLG.

We now turn to the BLG region of our heterostructure that is also covered by the MoS_2 top gate. The BLG in our heterostructure was produced by a "tear-and-stack" technique (Section S1 of the Supporting Information) which resulted in a small twist angle (estimated to be ∼0.02°) between the layers and a large Moiré pattern. Atomic relaxation leads to the formation of larger domains of Bernal bilayer graphene separated by domain walls[32] that host topological states.[8−10] The change in optical conductivity arising from the topological states reflects plasmon polaritons leading to fringes in nano-infrared experiments.[33,34] Changing the carrier density and interlayer bias across the BLG changes the optical conductivity across the domain wall and modifies the fringe pattern.[33] Figure 3B shows the nano-infrared amplitude over a region containing several domain walls for V_{bg} = +80 V and V_{tg} = 0 V. We observe features in the amplitude that correspond to plasmons reflecting off the domain walls.[34,35] As we increase V_{tg}, we observe a clear change in the plasmonic pattern that confirms the changing carrier density and interlayer bias in the BLG layer. By demonstrating dual gating and observing propagation of plasmons, we have thus shown the feasibility of performing nano-infrared studies of a dual gated system using this approach.

Next, we discuss the limitations of the TMD top gate. First, we consider the performance of the top gate at a negative V_{bg}. Because of the high work function of MoS_2, evaporated metals typically make n-type contact to MoS_2.[36] The geometry of our device is such that the titanium metal contacts to the MoS_2 lie outside the graphene region (Figure 1A). Therefore, the contact resistance at the Ti/MoS_2 layer depends only on V_{bg}. At a large negative V_{bg}, the Schottky barrier at the Ti/MoS_2 junction is too large and renders the top gate ineffective. Therefore, unless doped by local gates,[37] the MoS_2 top gate is only functional for positive V_{bg} where n-type carriers are injected into the MoS_2 layer.

At a fixed, positive V_{bg}, the region by the contacts remains n-doped and the application of V_{tg} starts to change the carrier

https://dx.doi.org/10.1021/acs.nanolett.0c04494
Nano Lett. 2021, 21, 1688−1693

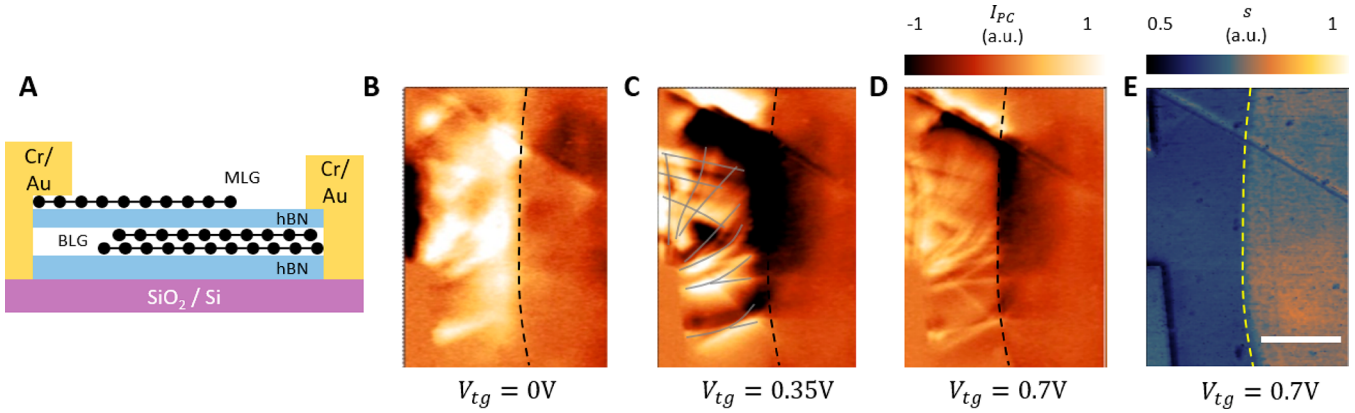

Figure 4. Monolayer graphene as a top gate for domain walls in bilayer graphene. (A) Schematic of the heterostructure. (B, C, D) Nano-photocurrent images for three different V_{tg} showing domain walls in the underlying bilayer graphene. (E) Nano-infrared amplitude image at V_{tg} = 0.7 V. Black dashed lines in panels B–D and yellow dashed line in panel E correspond to the boundary of the top-gated region. Gray solid lines in panel C indicate the domain walls in BLG. Scale bar, 1 μm.

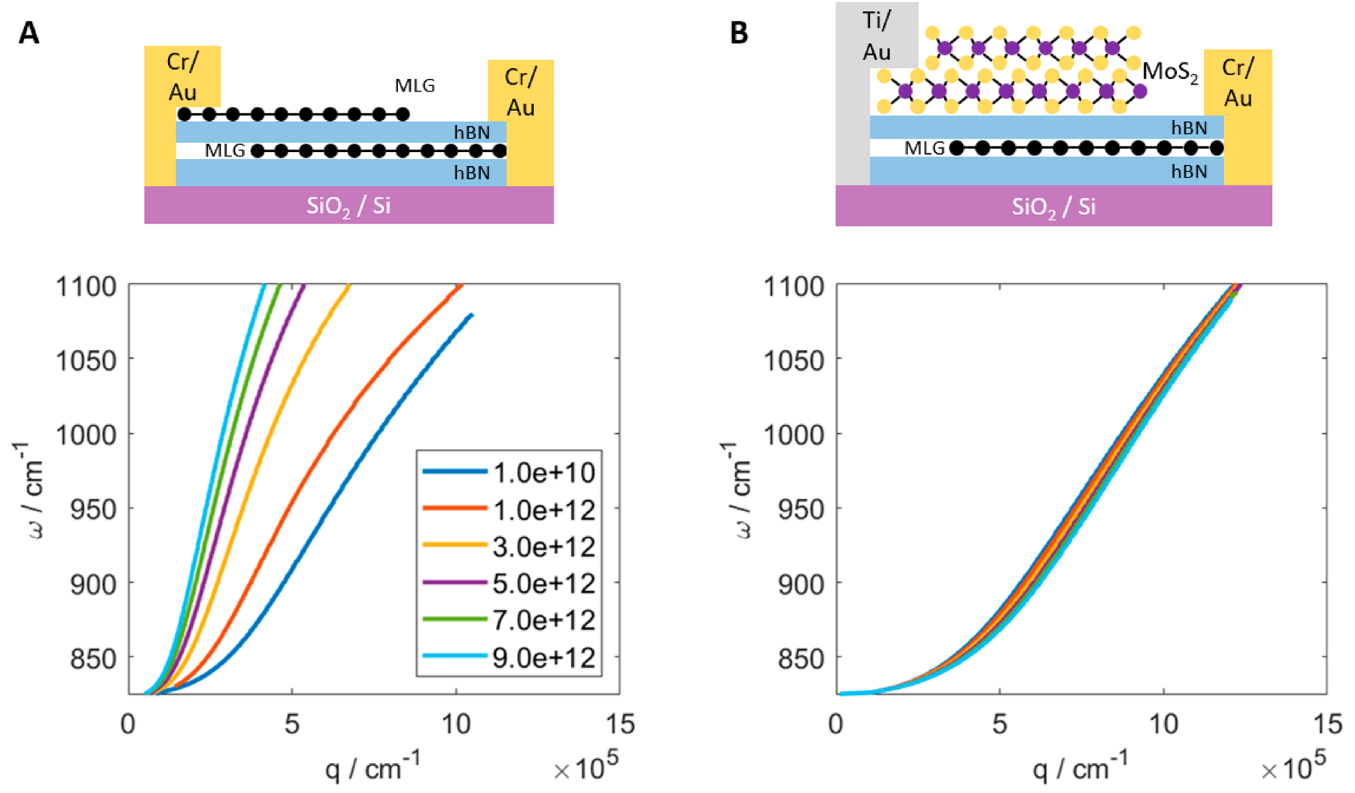

Figure 5. Direct comparison between the MLG and TMD top gates. (A) Change in the dispersion of the plasmonic mode of the heterostructure as the carrier density in the top gate is varied for a MLG top gate. (B) Similar plot as that of panel A for bilayer MoS_2 top gate. The thicknesses of the top and bottom hBNs are 5 and 30 nm, respectively, and the underlying MLG layer is doped to $n = 6 \times 10^{12}$ cm^{-2}.

density in the MoS_2 region directly above the graphene layer. When V_{tg} is negative, the carriers in the MoS_2 layer are all n-type. However, as V_{tg} becomes positive, the MoS_2 region above the graphene becomes hole-like. Since the carriers close to the contacts remain electron-like, a pn-junction forms in the MoS_2 layer along the graphene edge. This pn-junction isolates the Ti contacts from the MoS_2 region above the graphene layer and causes the top gate to become ineffective. Taking the effects of the Schottky barrier and the pn-junction together, we conclude that the top gate is most effective only in one of the four quadrants in the V_{tg}–V_{bg} plane and its performance decays quickly in the other quadrants, as illustrated in the inset of Figure 2B.

To achieve full control over the properties of BLG, we could consider other materials as a top gate. While a p-type TMD such as WS_2 can lead to a top gate that is functional at negative V_{bg}, the pn-junction limitation would still restrict its functionality to just one quadrant in the V_{bg}–V_{tg} plane. This limitation arises directly because of the electronic band gap and therefore would be present for any semiconductor. Only a gapless ambipolar material, such as monolayer graphene, can overcome this limitation.

https://dx.doi.org/10.1021/acs.nanolett.0c04494
Nano Lett. 2021, 21, 1688–1693

We now explore the possibility of using monolayer graphene (MLG) as a top gate for BLG. The ambipolar nature of MLG means that the contacts do not restrict the range of operational gate voltages. However, MLG has a strong optical response of its own in mid-infrared frequencies. At the same time, if the Fermi energy in the top-gate layer is very small, interband transitions in the top-gate layer will lead to an increased damping that can obscure the plasmonic features in nano-infrared imaging (Section S4.1 of the Supporting Information). Therefore, we also explored the nano-photocurrent technique which can selectively probe the underlying BLG layer.

Figure 4A shows a schematic of our heterostructure with a MLG top gate. Figure 4E shows the nano-infrared amplitude image of our device with V_{bg} = $_0$ V and V_{tg} = +0.7 V. The yellow dashed line indicates the boundary of the MLG top gate. We observe a nano-infrared contrast indicating that the top gate is active, but we see no other features, most likely because the carrier density in the bilayer graphene is too low (Section S1.4 of the Supporting Information). Panels A–D of Figure 4 show the results of nano-photocurrent experiments[38] at different V_{tg}. As V_{tg} is increased from zero, the nano-photocurrent begins to resemble the photocurrent profiles seen in other twisted BLG heterostructures[39,40] and are known to arise from domain walls. On the basis of the periodicity of the Moiré pattern, we estimate a twist angle of ∼0.1°. The irregularity of the domain wall pattern in Figure 4 in comparison to Figure 3 is due to strain accumulated during the fabrication process. These results demonstrate that we are able to resolve the domain wall pattern in nano-photocurrent through a doped MLG top gate.

Finally, we directly compare the properties of MLG and bilayer MoS_2 top gates for nano-infrared experiments with the following hypothetical scenario. We consider an encapsulated heterostructure of monolayer graphene with a carrier density of $n = 6 \times 10^{12}$ cm^{-2} with either a MLG top gate (Figure 5A) or a TMD top gate (Figure 5B). We then vary the carrier concentration only in the top gate to observe how strongly the top gate modifies the behavior of the underlying graphene layer. The plasmonic dispersions in both cases are shown in Figure 5. The dispersion changes significantly with a MLG top gate while it remains mostly unchanged in the case of the TMD top gate. The large change in the dispersion with the MLG top gate is due to strong hybridization between the plasmonic modes in the two graphene layers.[41−43] The smaller change in dispersion with a TMD top gate demonstrates that the hybridization of the plasmonic modes is negligible with a TMD top gate. The thickness of the TMD top gate leads to a small but significant effect on the plasmonic dispersion, as discussed in Section S5 of the Supporting Information. These results suggest that a TMD top gate allows direct access to the plasmonic phenomena in the underlying graphene layer in nano-infrared experiments with minimal obscuring.

In conclusion, our results demonstrate two near-field compatible top gates for BLG. With MoS_2, we were able to study plasmons through scattering nano-infrared experiments and demonstrate the depletion of carriers in the underlying graphene layers. With a MLG top gate, we were able to visualize the domain walls in the underlying BLG through nano-photocurrent experiments. Our work paves the way for exploring the plasmonic properties of gapped bilayer graphene with scanning nano-infrared and nano-photocurrent experiments.

■ ASSOCIATED CONTENT

Supporting Information

The Supporting Information is available free of charge at https://pubs.acs.org/doi/10.1021/acs.nanolett.0c04494.

Methods, nano-infrared images at different top-gate voltages, line profile fits using the damped oscillations model, nano-infrared vs nano-photocurrent with an MLG top gate, thickness dependence of the MoS_2 top gate, and gating of bilayer graphene with MoS_2 (PDF)

■ AUTHOR INFORMATION

Corresponding Author

D. N. Basov − *Department of Physics, Columbia University, New York 10027, United States*; Email: db3056@columbia.edu

Authors

Sai S. Sunku − *Department of Physics and Department of Applied Physics and Applied Mathematics, Columbia University, New York 10027, United States*; orcid.org/0000-0002-7037-8717

Dorri Halbertal − *Department of Physics, Columbia University, New York 10027, United States*; orcid.org/0000-0002-1665-0724

Rebecca Engelke − *Department of Physics, Harvard University, Cambridge, Massachusetts 02138, United States*

Hyobin Yoo − *Department of Physics, Harvard University, Cambridge, Massachusetts 02138, United States*; orcid.org/0000-0002-8039-9482

Nathan R. Finney − *Department of Mechanical Engineering, Columbia University, New York 10027, United States*

Nicola Curreli − *Department of Mechanical Engineering, Columbia University, New York 10027, United States*

Guangxin Ni − *Department of Physics, Columbia University, New York 10027, United States*; orcid.org/0000-0002-7216-1829

Cheng Tan − *Department of Mechanical Engineering, Columbia University, New York 10027, United States*

Alexander S. McLeod − *Department of Physics, Columbia University, New York 10027, United States*

Chiu Fan Bowen Lo − *Department of Physics, Columbia University, New York 10027, United States*

Cory R. Dean − *Department of Physics, Columbia University, New York 10027, United States*

James C. Hone − *Department of Mechanical Engineering, Columbia University, New York 10027, United States*

Philip Kim − *Department of Physics, Harvard University, Cambridge, Massachusetts 02138, United States*

Complete contact information is available at: https://pubs.acs.org/10.1021/acs.nanolett.0c04494

Author Contributions

[#]S.S.S. and D.H. contributed equally to this work.

Notes

The authors declare no competing financial interest.

■ ACKNOWLEDGMENTS

Research in van der Waals heterostructures at Columbia was solely supported as part of Programmable Quantum Materials, an Energy Frontier Research Center funded by the U.S. Department of Energy (DOE), Office of Science, Basic Energy Sciences (BES), under Award DE-SC0019443. D.N.B. is the

https://dx.doi.org/10.1021/acs.nanolett.0c04494
Nano Lett. 2021, 21, 1688−1693

Vannevar Bush Faculty Fellow (N00014-19-1-2630) and Moore Investigator in Quantum Materials EPIQS No. 9455. D.H. was supported by a fellowship from the Simons Foundation (579913). The work at Harvard was supported by NSF DMREF (Grant DMR-1922172). N.R.F. acknowledges support from the Stewardship Science Graduate Fellowship program provided under Cooperative Agreement No. DE-NA0003864. N.C. acknowledges the project SONAR, which has received funding from the European Union's Horizon 2020 research and innovation programme under the Marie Skłodowska−Curie Grant Agreement (No. 734690).

REFERENCES

(1) Fei, Z.; et al. Gate-tuning of graphene plasmons revealed by infrared nano-imaging. *Nature* **2012**, *487*, 82−85.
(2) Chen, J.; et al. Optical nano-imaging of gate-tunable graphene plasmons. *Nature* **2012**, *487*, 77−81.
(3) Ni, G. X.; et al. Fundamental limits to graphene plasmonics. *Nature* **2018**, *557*, 530−533.
(4) Low, T.; et al. Polaritons in layered two-dimensional materials. *Nat. Mater.* **2017**, *16*, 182−194.
(5) Li, G.; et al. Observation of Van Hove singularities in twisted graphene layers. *Nat. Phys.* **2010**, *6*, 109−113.
(6) Bistritzer, R.; MacDonald, A. H. Moire bands in twisted double-layer graphene. *Proc. Natl. Acad. Sci. U. S. A.* **2011**, *108*, 12233−7.
(7) Hunt, B.; et al. Massive dirac fermions and hofstadter butterfly in a van der Waals heterostructure. *Science* **2013**, *340*, 1427−1430.
(8) Martin, I.; Blanter, Y. M.; Morpurgo, A. F. Topological confinement in bilayer graphene. *Phys. Rev. Lett.* **2008**, *100*, 036804.
(9) Qiao, Z.; Jung, J.; Niu, Q.; MacDonald, A. H. Electronic highways in bilayer graphene. *Nano Lett.* **2011**, *11*, 3453−3459.
(10) Ju, L.; et al. Topological valley transport at bilayer graphene domain walls. *Nature* **2015**, *520*, 650−655.
(11) Cao, Y.; et al. Correlated Insulator Behaviour at Half-Filling in Magic Angle Graphene Superlattices. *Nature* **2018**, *556*, 80−84.
(12) Cao, Y.; et al. Unconventional superconductivity in magic-angle graphene superlattices. *Nature* **2018**, *556*, 43−50.
(13) Basov, D. N.; Fogler, M. M.; Lanzara, A.; Wang, F.; Zhang, Y. Colloquium: Graphene spectroscopy. *Rev. Mod. Phys.* **2014**, *86*, 959−994.
(14) Fei, Z.; et al. Infrared nanoscopy of dirac plasmons at the graphene-SiO2interface. *Nano Lett.* **2011**, *11*, 4701−4705.
(15) Jablan, M.; Buljan, H.; Soljačić, M. Plasmonics in graphene at infrared frequencies. *Phys. Rev. B: Condens. Matter Mater. Phys.* **2009**, *80*, 254435.
(16) Basov, D. N.; Fogler, M. M.; García De Abajo, F. J. Polaritons in van der Waals materials. *Science* **2016**, *354* (6309), aag1992.
(17) Basov, D. N.; Asenjo-Garcia, A.; Schuck, P. J.; Zhu, X.; Rubio, A. Polariton panorama. *Nanophotonics* **2020**, *10*, 549−577.
(18) Woessner, A.; et al. Highly confined low-loss plasmons in graphene-boron nitride heterostructures. *Nat. Mater.* **2015**, *14*, 421−425.
(19) Fei, Z.; et al. Tunneling Plasmonics in Bilayer Graphene. *Nano Lett.* **2015**, *15*, 4973−4978.
(20) Low, T.; Chen, P. Y.; Basov, D. N. Superluminal plasmons with resonant gain in population inverted bilayer graphene. *Phys. Rev. B: Condens. Matter Mater. Phys.* **2018**, *98*, 041403.
(21) Hasdeo, E. H.; Song, J. C. W. Long-Lived Domain Wall Plasmons in Gapped Bilayer Graphene. *Nano Lett.* **2017**, *17*, 7252−7257.
(22) Chen, G.; et al. Signatures of tunable superconductivity in a trilayer graphene moiré superlattice. *Nature* **2019**, *572*, 215−219.
(23) Liu, X.; et al. Tunable spin-polarized correlated states in twisted double bilayer graphene. *Nature* **2020**, *583*, 221−225.
(24) Kerelsky, A.; et al. Moiréless correlations in ABCA graphene. *Proc. Natl. Acad. Sci. U. S. A.* **2021**, *118*, No. e2017366118.
(25) Oostinga, J. B.; Heersche, H. B.; Liu, X.; Morpurgo, A. F.; Vandersypen, L. M. K. Gate-induced insulating state in bilayer graphene devices. *Nat. Mater.* **2008**, *7*, 151−157.
(26) Zhang, Y.; et al. Direct observation of a widely tunable bandgap in bilayer graphene. *Nature* **2009**, *459*, 820−823.
(27) Yan, H.; et al. Tunable infrared plasmonic devices using graphene/insulator stacks. *Nat. Nanotechnol.* **2012**, *7*, 330−334.
(28) Ju, L.; et al. Tunable excitons in bilayer graphene. *Science* **2017**, *358*, 907−910.
(29) Li, H.; et al. Global Control of Stacking-Order Phase Transition by Doping and Electric Field in Few-Layer Graphene. *Nano Lett.* **2020**, *20*, 3106−3112.
(30) Ocelic, N.; Huber, A.; Hillenbrand, R. Pseudoheterodyne detection for background-free near-field spectroscopy. *Appl. Phys. Lett.* **2006**, *89*, 101124.
(31) Fei, Z.; et al. Electronic and plasmonic phenomena at graphene grain boundaries. *Nat. Nanotechnol.* **2013**, *8*, 821−825.
(32) Yoo, H.; et al. Atomic and electronic reconstruction at the van der Waals interface in twisted bilayer graphene. *Nat. Mater.* **2019**, *18*, 448−453.
(33) Jiang, B. Y.; et al. Plasmon Reflections by Topological Electronic Boundaries in Bilayer Graphene. *Nano Lett.* **2017**, *17*, 7080−7085.
(34) Sunku, S. S.; et al. Photonic crystals for nano-light in moiré graphene superlattices. *Science* **2018**, *362*, 1153−1156.
(35) Jiang, B. Y.; et al. Tunable Plasmonic Reflection by Bound 1D Electron States in a 2D Dirac Metal. *Phys. Rev. Lett.* **2016**, *117*, 086801.
(36) Liu, Y.; et al. Approaching the Schottky-Mott limit in van der Waals metal-semiconductor junctions. *Nature* **2018**, *557*, 696−700.
(37) Jauregui, L. A.; et al. Electrical control of interlayer exciton dynamics in atomically thin heterostructures. *Science* **2019**, *366*, 870−875.
(38) Woessner, A.; et al. Near-field photocurrent nanoscopy on bare and encapsulated graphene. *Nat. Commun.* **2016**, *7*, 10783.
(39) Sunku, S. S.; et al. Hyperbolic enhancement of photocurrent patterns in minimally twisted bilayer graphene. *arXiv (Condensed Matter: Mesoscale and Nanoscale Physics)*, 2020. arXiv:2011.05179. http://arxiv.org/abs/2011.05179 (accessed 2021-01-27).
(40) Hesp, N. C. H.; et al. Nano-imaging photoresponse in a moire unit cell. *arXiv (Condensed Matter: Mesoscale and Nanoscale Physics)*, 2020. arXiv:2011.05060. http://arxiv.org/abs/2011.05060 (accessed 2021-01-27).
(41) Das Sarma, S.; Madhukar, A. Collective modes of spatially separated, two-component, two-dimensional plasma in solids. *Phys. Rev. B: Condens. Matter Mater. Phys.* **1981**, *23*, 805−815.
(42) Profumo, R. E. V.; Asgari, R.; Polini, M.; MacDonald, A. H. Double-layer graphene and topological insulator thin-film plasmons. *Phys. Rev. B: Condens. Matter Mater. Phys.* **2012**, *85*, 085443.
(43) Stauber, T.; Gómez-Santos, G. Plasmons and near-field amplification in double-layer graphene. *Phys. Rev. B: Condens. Matter Mater. Phys.* **2012**, *85*, 075410.

https://dx.doi.org/10.1021/acs.nanolett.0c04494
Nano Lett. 2021, 21, 1688−1693